remote sensing

MDPI

Communication

Icequakes and Large Shear Wave Velocity Drop in the Kuoqionggangri Glacier of Tibetan Plateau Observed with Fiber Optic Seismometer Array

Yanan Li [1,2], Wenzhu Huang [3], Guohui Li [4], Wei Yang [1], Xiaolong Zhang [1], Jiule Li [1], Wentao Zhang [3] and Baiqing Xu [1,5,*]

[1] State Key Laboratory of Tibetan Plateau Earth System, Environment and Resources (TPESER), Institute of Tibetan Plateau Research, Chinese Academy of Sciences, Beijing 100101, China
[2] University of Chinese Academy of Sciences, Beijing 100049, China
[3] State Key Laboratory of Transducer Technology, Institute of Semiconductors, Chinese Academy of Sciences, Beijing 100083, China
[4] Key Laboratory of Earthquake Prediction, Institute of Earthquake Forecasting, China Earthquake Administration, Beijing 100036, China
[5] CAS Center for Excellence in Tibetan Plateau Earth Sciences, Beijing 100101, China
* Correspondence: baiqing@itpcas.ac.cn

Abstract: We developed a kind of fiber optic seismometer array for a high mountain glacier and first tested it on the Kuoqionggangri Glacier in the Tibetan Plateau. The array clearly recorded substantial passive seismic source signals of various icequakes, including shallow, deep and hybrid events. These fracturing activities indicate that crevasses and/or fractures developed in the glacier. We further obtained the glacial thickness of about 40 m by analyzing the active seismic source after hitting the glacier surface with a hammer based on the seismic scattering method. Most importantly, we observed a low shear wave velocity layer with a large velocity drop of ~28% and thickness of about ~7 m in the lower glacier. It is inferred that the low-velocity layer may represent a temperate ice layer. Our experiment provides a kind of feasible seismic observation to study icequakes and the englacial structure of Tibetan glaciers, offering new insights for evaluating glacier change in the Tibetan Plateau.

Keywords: fiber optic seismometer; icequake; glacial structure; temperate ice; Kuoqionggangri Glacier; Tibetan Plateau

Citation: Li, Y.; Huang, W.; Li, G.; Yang, W.; Zhang, X.; Li, J.; Zhang, W.; Xu, B. Icequakes and Large Shear Wave Velocity Drop in the Kuoqionggangri Glacier of Tibetan Plateau Observed with Fiber Optic Seismometer Array. *Remote Sens.* **2023**, *15*, 1282. https://doi.org/10.3390/rs15051282

Academic Editor: Ian Brown

Received: 24 January 2023
Revised: 18 February 2023
Accepted: 22 February 2023
Published: 25 February 2023

1. Introduction

Since the 1960s, the glaciers in the Tibetan Plateau (TP) have experienced a markedly rapid retreat and accelerated melting with climate warming [1–3], leading to accelerated glacial mass loss [2,4], glacier surging and avalanches [5–7]. These changes have produced profound challenges for human activity [8–11]. The thermal regime and hydraulic conditions of a mountain glacier controls its flow rheology and basal conditions affecting glacier dynamics, which in turn affect its behaviour in response to climate change. Icequakes and glacial structure can provide essential constraints for the thermal and hydrous states of glaciers.

Seismic observations have been broadly applied to study icequakes and glacial structure in the Alps, Himalayas, Alaska, Greenland and Antarctica [12–22]. These studies observed various shallow and deep icequakes, englacial low seismic velocity, fluid resonance and tremors, which were generally explained to be related to temperature and/or water. Until now, there have still been relatively few seismic observations in the glaciers of the TP, namely, a few icequake observations using sparse traditional broadband [23] and short-period [24,25] seismometers.

With the rapid development of fiber optic sensor and photoelectron technologies, fiber optic seismometers were born [26–28]. Compared with traditional seismometers, they use

optical fiber as the sensing and signal transmission medium without any electronic devices, and can work stably for a long time in an extremely low temperature and underwater environment. What is more, fiber optic seismometers are relatively inexpensive for high-resolution seismic observation. There are two main kinds of fiber optic seismometers, namely, distributed optical fiber acoustic sensing (DAS) and fiber optic seismometer array (FOSA). DAS systems typically measure the high-density distributed strain or strain rate along a fiber optic cable. This technology inputs laser pulses into an optical cable, and measure optical phase changes in Rayleigh backscattered light. It requires the particle strain–velocity conversion model for the study of underground velocity structure, which would produce some errors [26,27]. FOSA consists of many Michelson fiber interferometers in series on one fiber optic cable, and interrogates the phase of each fiber interferometer by laser. Compared with the DAS, the FOSA can directly measure single-component or three-component acceleration seismic waves without needing the particle velocity conversion model, and has a lower noise level [28]. The DAS and FOSA have been broadly applied to study continental shallow structure and earthquakes [28–33]. Recently, there have also been many reports about the DAS being used to detect glacial structure and seismicity [34–38]. Related research regarding the FOSA has not been performed.

We carried out an experimental observation using the dense FOSA on the Kuoqionggangri (KQGR) Glacier in the TP on 7 August 2021 (Figure 1). The KQGR glacier is located at the southern TP, with an elevation of 5540–5840 m and area of 1.02 km^2. Its surface melted significantly and developed many marginal lakes (Figure 1c). The FOSA worked well in the extreme high mountain environment with low temperature and atmospheric pressure. We obtained high-quality records at 16 seismometers with high-frequency sampling of 1000 Hz. There are substantial passive source signals of shallow and deep icequakes with different spectrum signatures in these records. Based on active source data from hitting the glacier surface with a hammer, we obtained the thickness and seismic velocity of the glacier using the seismic scattering method [39,40]. These results provide new observational evidences for the glacial activity and englacial structure anomaly related to temperature and water in the TP.

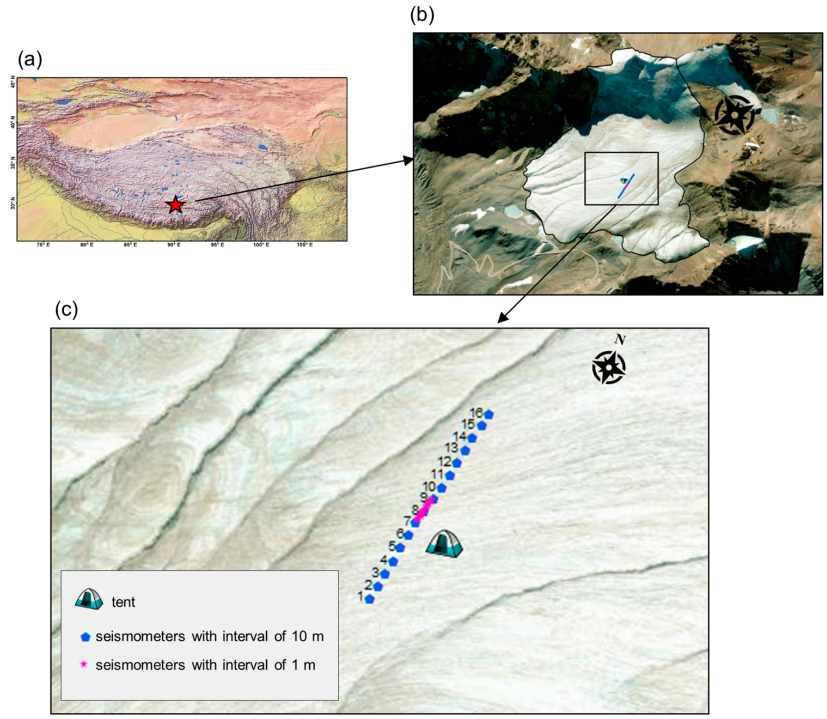

Figure 1. The installed FOSA consisting of 16 seismometers on the KQGR Glacier in the TP. (**a**) The study area. The red star marks the location of the KQGR Glacier. (**b**) The KQGR Glacier. The black box shows the location of the installed seismometers. (**c**) The installed 16 seismometers. The blue and pink pentagons are the seismometers with intervals of 10 m and 1 m, respectively.

2. Seismic Observations

2.1. Fiber Optic Seismometer Array

We developed a kind of FOSA, which consists of 16 fiber optic seismometers. Each seismometer is connected by a 25 m 16-core single-mode optical cable. The seismometer is an all-metal optic fiber accelerometer based on an optic fiber Michelson interferometer and double diaphragm structure [41]. The acceleration sensitivity of the accelerometer is calibrated by a standard shake table. The seismometer has a flat sensitivity response, and good sensitivity consistency. The sensitivity of the seismometer is about 41 dB (re: 0 dB = 1 rad/g) with a fluctuation less than $\pm$1.5 dB within the frequency range from 1 to 500 Hz. The seismometer is vertical with a tilt tolerance of 25°. Its metal shell has good sealing performance. The seismometer can be directly used in underwater or glacial melt water and has a wide working temperature range from -80 °C to above 100 °C.

The signal interrogator of the FOSA is based on the optic interferometric phase demodulation method and phase generation carrier (PGC) algorithm [42]. The phase noise level is about 118 dB @5 Hz (1.26×10^{-6} rad/$\sqrt{\text{Hz}}$ @5 Hz), which is two or three orders of magnitude better than the DAS. The system noise level is about 12.6 ng/$\sqrt{\text{Hz}}$ @5 Hz considering the sensitivity of FOSA. The working principle of the FOSA is as follows: When an external seismic wave or environmental background noise acts on the FOSA, the inertial structure of each optic fiber accelerometer vibrates and deforms the internal dual-diaphragm structure. Then the optic fiber interferometer wrapped on the dual-diaphragm structure produces deformation and phase output. We can obtain the external vibration acceleration signal by measuring the phase change in the optic fiber interferometer through the optic fiber signal interrogator because the phase output of the fiber optic seismometer is linear with the external acceleration.

2.2. Seismic Array Layout

The FOSA including 16 fiber optic seismometers was installed in a line with seismometer intervals of 10 and 1 m on the KQGR Glacier (Figure 1c). The seismometers were buried underneath the glacier surface with a depth of about 30 cm (Figure 2a). The seismic array was designed along the direction of the glacier flowline with a tent in the middle part (Figure 2b). The data collector and battery were placed in the tent. To avoid the effects of the vibration of the engine on the seismic signal recording, we used a 12 V battery to power the data collector. The total observed time lasted for about 40 h.

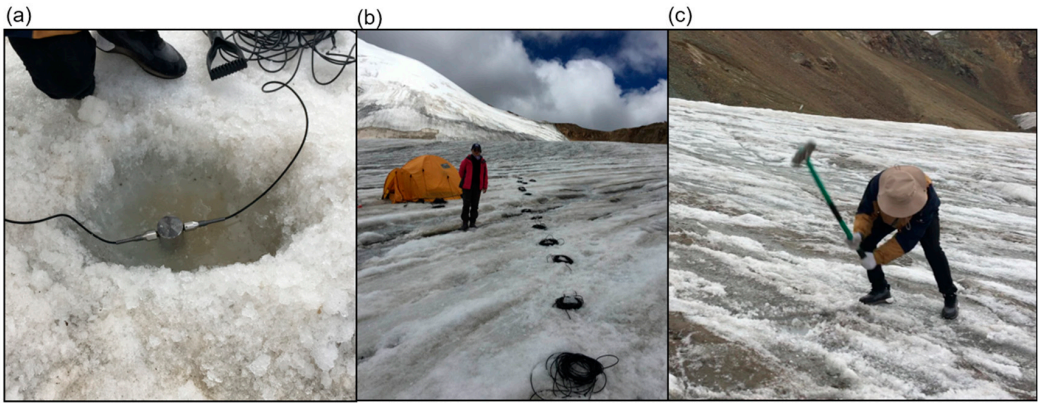

Figure 2. Field photos of seismic observations with the fiber optic seismometers on the KQGR Glacier. (**a**) A buried seismometer in the ice. (**b**) Installed seismic array. (**c**) Producing active seismic source by hitting the ice surface using a heavy hammer.

To study the glacial structure, active seismic sources were generated by hitting the glacier surface for 20 times using a heavy hammer of 7 kg (Figure 2c). The sources were arranged in a line with the seismic array. For the observation of the seismometer interval

of 10 m, the sources were set as 15 m, 30 m and 50 m away from the seismometer No. 1. For 1 m, the distances between the sources and the seismometer No. 1 were 20 m and 50 m.

2.3. Seismic Records

2.3.1. Passive Seismic Source

We obtained seismograms with high signal to noise ratios recorded by the FOSA. Substantial icequakes were observed with greatly different waveforms, suggesting a variety of possible source mechanisms.

Numerous shallow icequakes occurred frequently and were visually identified. Figure 3a exhibits an example of the seismograms with lasting time of 0.6 s. There were at least five visible shallow icequakes (marked by orange shadows in the Figure 3a) that occurred with time intervals varying from about 0.05 s to 0.23 s. The lasting times for these icequakes were extremely short, no more than 0.03 s. Their waveforms were similar and dominated by obvious low-frequency Rayleigh waves.

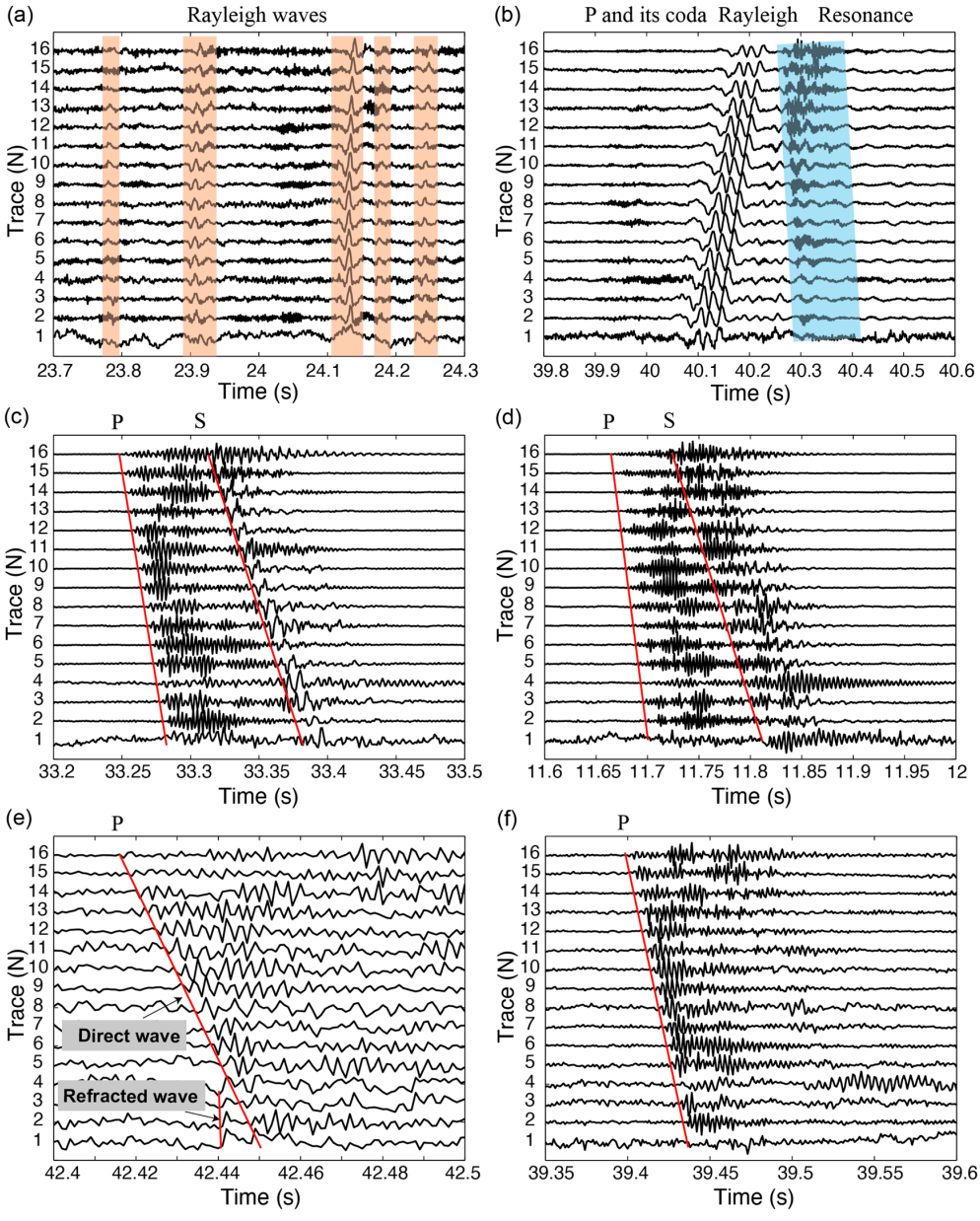

Figure 3. Vertical seismograms of different types of icequakes recorded by the 16 fiber optic seismometers with intervals of 10 m. (**a**) Seismic waveforms of a shallow icequake. (**b**) Seismic waveforms of a hybrid

icequake. (**c**–**f**) Seismic waveforms of four deep icequakes. The waveforms are normalized by individual largest amplitudes. The origin times of seismograms are 23.7 s at 01:26 a.m. (**a**), 39.8 s at 04: 43 a.m. (**b**), 33.2 s at 01:55 a.m. (**c**), 11.6 s at 04:42 a.m. (**d**), 42.4 s at 04:42 a.m. (**e**) and 39.35 s at 01:43 a.m. (**f**) on 8 August 2021 in Beijing time.

Figure 3b shows another type of shallow icequake whose lasting time was longer. There were higher frequency P waves and its codas had weak energies before the low-frequency Rayleigh waves. Moreover, there was a resonance of the obvious low-frequency monochromatic coda lasting for about 0.4 s after the Rayleigh wave, indicating that this event was a hybrid icequake [18]. In addition, there was another icequake after the hybrid event, shown with blue shadow in Figure 3b.

We also observed many different types of deep icequakes (Figure 3c–f). They featured impulsive P and/or S waves and did not have a notable Rayleigh phase. The deep icequakes in Figure 3c,d both lasted about 1.5 s and had obvious S phases but different S waveforms. The S waves for the deep icequakes in Figure 3e,f were obscure. These two icequakes lasted no more than 0.1 s.

There were obvious refracted waves of ice–rock interface that arrived first before direct P waves for the icequake in the Figure 3e. The refracted waves traveled downward first, then refracted at the ice–rock interface, and finally traveled up toward the receiver. Due to the higher velocity of rock than ice, the refracted waves arrived first before the direct waves traveling in ice only (directly from source to receiver) when the epicentral distance increased to a critical value. Therefore, the existence of the refracted waves may indicate that it was an intermediate-deep icequake.

2.3.2. Active Seismic Source

Figure 4 shows the seismograms with active source generated by the hammer hitting. Their waveforms lasted about 0.1 s. The onsets of the direct P wave are clearly recorded. The polarities of the P waves are downward, which is consistent with the directions of the hammer hitting.

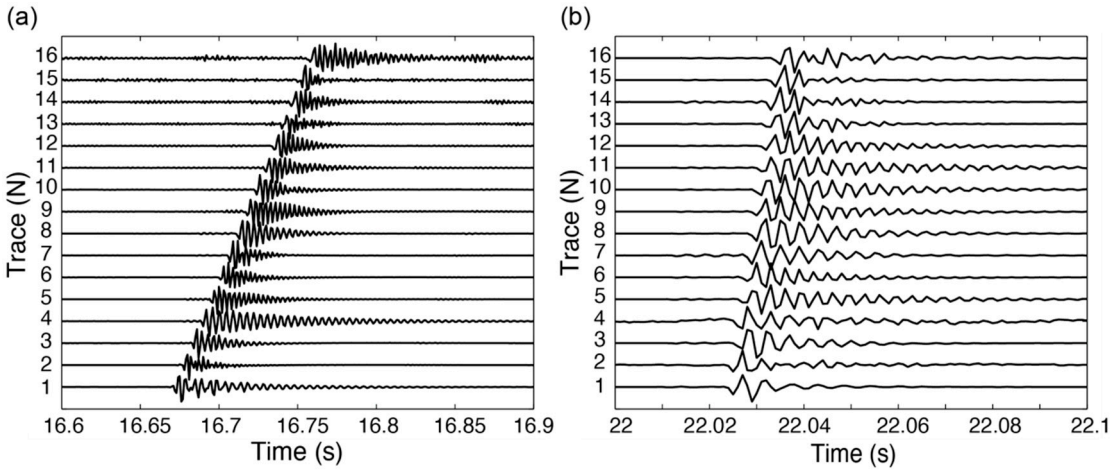

Figure 4. Vertical normalized seismograms of the hammer hitting recorded by the 16 fiber optic seismometers with intervals of 10 m (**a**) and 1 m (**b**). The offsets between the seismic source of hammer hitting and the seismometer No. 1 are 15 m in (**a**) and 50 m in (**b**). The origin times of seismograms are 16.6 s at 12:36 p.m. on 8 August (**a**) and 22.0 s at 11:47 a.m. (**b**) on 9 August 2021 in Beijing time.

3. Seismic Waveform Analyses

3.1. Spectral Analysis

Different types of icequakes have different seismic sources and spectrum features [20]. We calculated the spectrograms of the seismic traces from the seismometers No. 2, 7 and 15 for the different types of icequakes. Although the energies for different frequencies may be affected by the response between the source and the receiver, these seismic traces generally show similar spectrum characteristics. Figure 5 shows the spectrograms from the seismometer No. 7. The main frequencies are less than 80 Hz for the shallow icequakes (Figure 5a,b). The seismograms of the deep icequakes (Figure 5c–f) show higher frequencies. The main frequencies of P wave and its coda wave are in the range of 300–400 Hz and 100–250 Hz for the S wave.

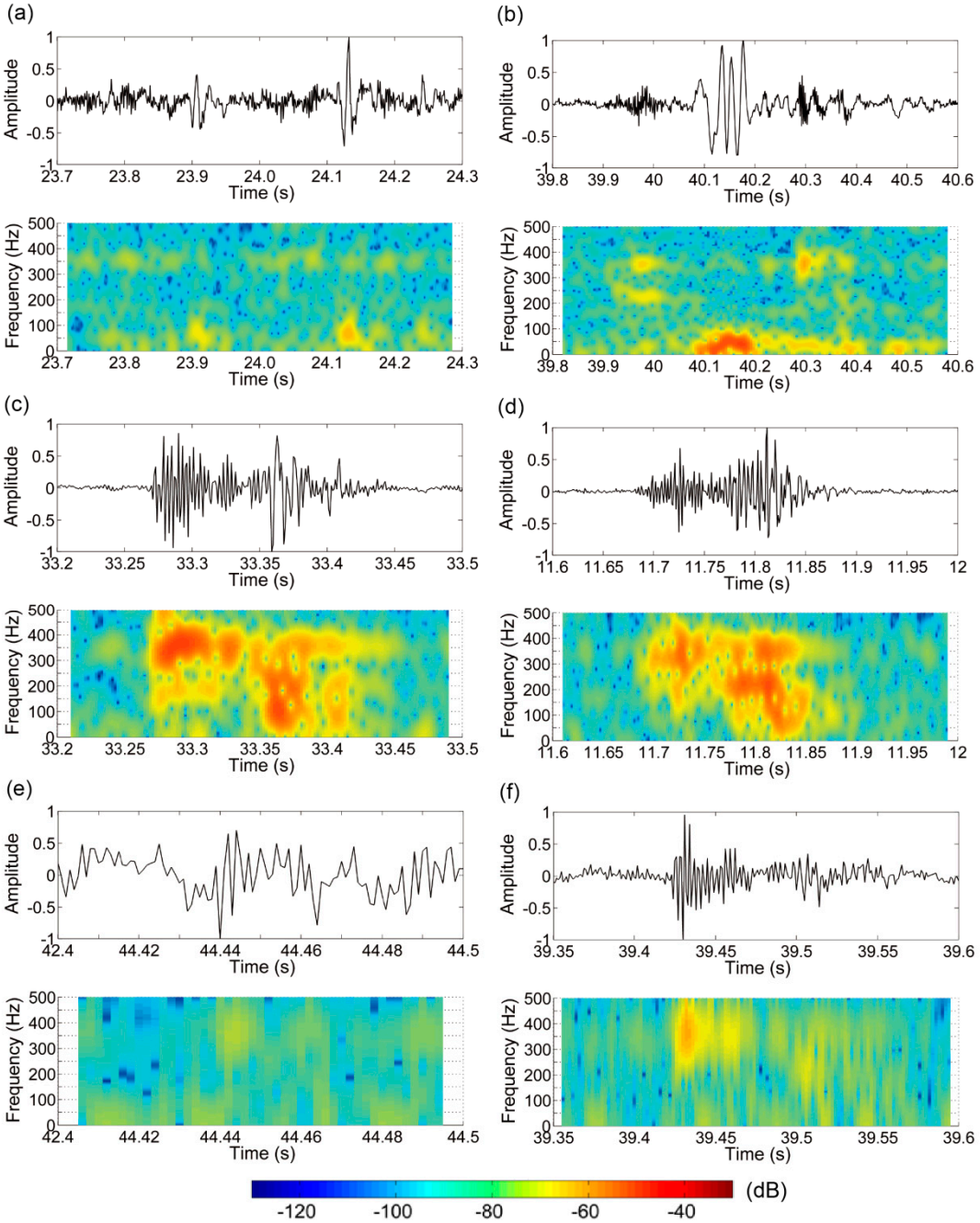

Figure 5. Spectrograms for the shallow (**a**), hybrid (**b**) and deep (**c**–**f**) icequakes from the seismometer No. 7. The origin times of the seismograms are the same as Figure 3.

3.2. Seismic Scattering Method

We used the seismic scattering profile (SSP) method [39,40] to image the velocity structure of the KQGR Glacier. The seismic signals were generated by using a heavy hammer to strike the ice surface. Seismic scattering and reflected waves are generated when seismic waves propagate in a heterogeneous medium. According to the seismic scattering theory, the seismic record is the isochronous superposition of the scattered signals in the ellipsoid between the seismic source and the receiver. Taking rays as a basic unit, the superposition energy maximization principle is used to determine scanning velocity, and then migration imaging is applied to obtain the underground velocity structure.

The SSP method mainly includes filtering, velocity scanning and migration imaging. Firstly, frequency-wavenumber filtering was used to reduce the effects of surface and sound waves, and enhance the energies of the englacial scattering and reflected waves. Secondly, Radon transform was applied to seismic velocity scanning. Integral transformation was performed along the hyperbolic path based on varied seismic velocities. When the seismic velocity is consistent with the real velocity, the energy of the scattered waves is the strongest. Finally, the synthetic aperture imaging based on the Kirchhoff integral was used to obtain the glacial velocity structure.

We obtained the seismic velocity structure of the KQGR Glacier in the TP for the two kinds of seismic arrays with intervals of 1 and 10 m, respectively. The results from the two seismic arrays show a similar glacial structure (Figure 6). There is a large velocity increment at a depth of about 40 m, depicting the ice–rock interface depth. The ice thickness model reveals a similar thickness of about 47 m, which is calculated based on the glacier surface motion and slope (Figure 7) [43]. Most importantly, our results reveal small-scale structure heterogeneity. A low-velocity layer is found at a depth of about 30 m with a thickness of about 7 m with a large S wave velocity drop of about 28%. A similar S wave velocity drop has also been observed at the polar ice sheets with a value of about 25% [19].

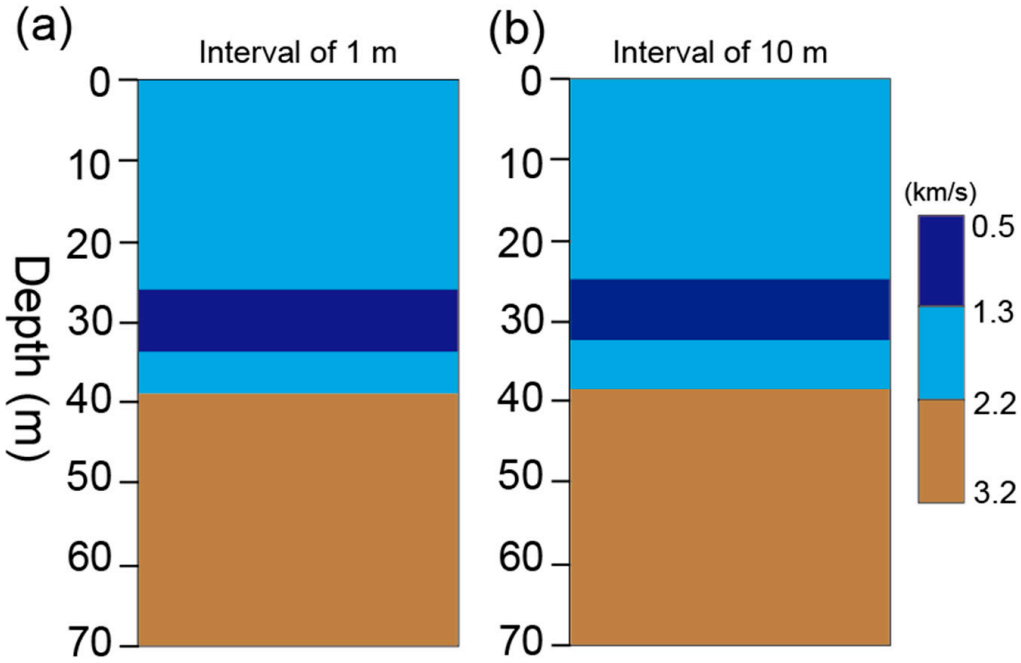

Figure 6. Estimated S wave velocity structure of the KQGR Glacier based on the seismograms from the 16 seismometers with intervals of 1 m (**a**) and 10 m (**b**).

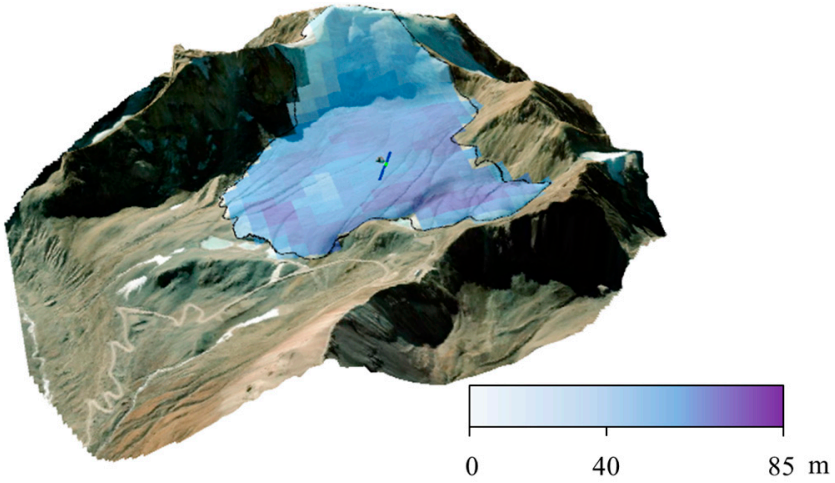

Figure 7. The thickness of the KQGR glacier calculated by glacier surface motion and slope.

4. Discussion

We observed many different types of icequakes including shallow, deep and hybrid events. Shallow icequakes are associated with ice surface crevasse opening or propagation [14,44], which is a valuable tool for assessing strain rates and changes thereof [20]. Their signals occupy the frequency range between 10 and 50 Hz [13,14,44–46], which are basically close to our observations. Previous studies suggested that near-surface icequakes constitute most short-duration seismic detections in high-melt areas [16,17]. Figure 3a shows an example also showing that the surface crevasse icequakes occurred frequently (at least 5 events in 0.6 s) on the high-melt KQGR Glacier.

We observed some resonances in the coda wave of some icequakes. Figures 3b and 5b show an example of a hybrid icequake that is characterized by high-frequency onset followed by a lower frequency monochromatic coda. Similar hybrid events were detected in the Alaska [47] and Alpine [18] glaciers. These events were explained as brittle fractures triggered by fluids, and the following resonances were induced by water rushing into a newly opened fracture.

We also detected many deep icequakes characterized by extremely high main frequencies of 300–400 Hz, which are much larger than the 100–200 Hz of most icequakes that occurred in Alpine, Greenland and Antarctica [16,18,20]. The deep icequakes can be divided into intermediate-deep and basal icequakes. The intermediate-depth icequakes are usually linked to hydraulic fracturing [18]. Basal icequakes are usually interpreted as the results of the opening or closing of tensile faults near the ice–rock interface induced by varied water pressure [48] or basal slip [49]. There is at least one intermediate-deep icequake identified by the obvious refracted waves (Figure 3e) among the four examples of deep icequakes. The existence of these intermediate-deep and/or basal icequakes in the KQGR Glacier indicates that water may play an important role in glacier activity.

Interestingly, we observed a low S wave velocity layer with a velocity drop of about 28% in the lower glacier. Such a strong decrease in the S wave velocity with depth cannot be explained by temperature change only [50]. The presence of water can explain the strong velocity drop [19,51,52]. The temperate ice is known as water-rich ice at the melting temperature at a given pressure [53,54]. Thus, the observed low-velocity layer may represent a temperate ice layer. A temperate ice layer was also found by GPR anomaly in the Jima Yangzong Glacier of the western Himalayas [53]. The existence of the temperate ice may shorten the timescale of the thermal regime change of the glacier in response to climate warming and accelerate the ice deformation rate [53,55], which would play an important role in the evolution of the glacier.

The meltwater on the KQGR Glacier surface is very rich during the summer season. Substantial shallow, deep and hybrid icequakes may indicate that crevasses and/or frac-

tures developed in the glacier. The surface meltwater of a glacier can be mostly routed to its interior through crevasses and moulins [55,56]. Given sufficient water supply, a water-filled fracture can propagate in the base of a glacier [57–60]. Valley-type mountain glaciers in cold climates are greatly affected by water percolation into crevassed fields, which release latent heat into the ice body [61]. Therefore, the temperate ice layer may be induced by the surface ice-melting water percolating through crevasses.

This experiment indicates that the FOSA can work well in the extreme high mountain environment with low temperature and atmospheric pressure, and can be used for dense seismic observations for icequakes and glacial structure. Because of the linearly distributed seismic array and the short observation period, we did not detect all the possible icequakes and locate them. Instead, we visually checked some of them. The time and space features of the icequakes will be further considered using more reasonably distributed seismometers with a longer observation in the future.

5. Conclusions

The fiber optic seismometers can work well in an extreme high mountain environment on the Kuoqionggangri Glacier in the Tibetan Plateau. We detected abundant various shallow, deep and hybrid icequakes with different spectrum features. The estimated thickness of the glacier is about 40 m. There is a low-velocity layer with an S wave velocity drop of 28% and thickness of about 7 m in the lower glacier, possibly indicating a temperate ice layer that may accelerate the glacier change rate in response to climate warming. These findings provide a new insight for assessing glacial deformation and dynamics in the Tibetan Plateau. This experiment also documented that our developed fiber optical seismometer is a feasible measuring method for glacier seismology.

Author Contributions: Conceptualization, Y.L. and B.X.; methodology, Y.L.; software, Y.L. and W.H.; validation, Y.L. and B.X.; formal analysis, Y.L. and G.L.; investigation, Y.L., W.H. and X.Z.; resources, B.X. and W.Z.; data curation, Y.L.; writing—original draft preparation, Y.L.; writing—review and editing, Y.L., W.H., G.L., W.Y., X.Z., J.L., W.Z. and B.X.; visualization, Y.L. and G.L.; supervision, B.X.; project administration, Y.L.; funding acquisition, B.X., J.L. and W.H. All authors have read and agreed to the published version of the manuscript.

Funding: This research was funded by the second Tibetan Plateau Scientific Expedition and Research Program, grant number 2019QZKK0101, the National Natural Science Foundation of China, grant number 42271312, U1939207, the Strategic Priority Research Program of Chinese Academy of Sciences, grant number XDA20070102, the Youth Innovation Promotion Association of CAS, grant number 2022110, the Scientific Instrument Developing Project of the Chinese Academy of Sciences, grant number YJKYYQ20210036 and the Science and Technology Program of Tibet Autonomous Region, grant number XZ202101ZD0014G.

Data Availability Statement: The data presented in this study are available on reasonable request from the corresponding author.

Acknowledgments: We thank the academic editor Maja Dragojevic and three anonymous reviewers for their constructive comments. We are grateful to the professor Evgeny A. Podolskiy for constructive suggestions, and the Beijing Tongdu Engineering Geophysical Prospecting Technology Co for some processes of seismic waveforms.

Conflicts of Interest: The authors declare no conflict of interest.

References

1. Yao, T.; Xue, Y.; Chen, D.; Chen, F.; Thompson, L.; Cui, P.; Koike, T.; Lau, W.K.-M.; Lettenmaier, D.; Mosbrugger, V.; et al. Recent Third Pole's Rapid Warming Accompanies Cryospheric Melt and Water Cycle Intensification and Interactions between Monsoon and Environment: Multidisciplinary Approach with Observations, Modeling, and Analysis. *Bull. Am. Meteor. Soc.* **2019**, *100*, 423–444. [CrossRef]
2. Bhattacharya, A.; Bolch, T.; Mukherjee, K.; King, O.; Menounos, B.; Kapitsa, V.; Neckel, N.; Yang, W.; Yao, T. High Mountain Asian Glacier Response to Climate Revealed by Multi-Temporal Satellite Observations since the 1960s. *Nat. Commun.* **2021**, *12*, 4133. [CrossRef] [PubMed]

3. Miles, E.; McCarthy, M.; Dehecq, A.; Kneib, M.; Fugger, S.; Pellicciotti, F. Health and Sustainability of Glaciers in High Mountain Asia. *Nat. Commun.* **2021**, *12*, 2868. [CrossRef] [PubMed]
4. Zhou, Y.; Li, Z.; Li, J.; Zhao, R.; Ding, X. Glacier Mass Balance in the Qinghai–Tibet Plateau and Its Surroundings from the Mid-1970s to 2000 Based on Hexagon KH-9 and SRTM DEMs. *Remote Sens. Environ.* **2018**, *210*, 96–112. [CrossRef]
5. Guillet, G.; King, O.; Lv, M.; Ghuffar, S.; Benn, D.; Quincey, D.; Bolch, T. A Regionally Resolved Inventory of High Mountain Asia Surge-Type Glaciers, Derived from a Multi-Factor Remote Sensing Approach. *Cryosphere* **2022**, *16*, 603–623. [CrossRef]
6. Vale, A.B.; Arnold, N.S.; Rees, W.G.; Lea, J.M. Remote Detection of Surge-Related Glacier Terminus Change across High Mountain Asia. *Remote Sens.* **2021**, *13*, 1309. [CrossRef]
7. Shugar, D.H.; Jacquemart, M.; Shean, D.; Bhushan, S.; Upadhyay, K.; Sattar, A.; Schwanghart, W.; McBride, S.; de Vries, M.V.W.; Mergili, M.; et al. A Massive Rock and Ice Avalanche Caused the 2021 Disaster at Chamoli, Indian Himalaya. *Science* **2021**, *373*, 300–306. [CrossRef]
8. Bolch, T. Asian Glaciers Are a Reliable Water Source. *Nature* **2017**, *545*, 161–162. [CrossRef]
9. Immerzeel, W.W.; van Beek, L.P.H.; Bierkens, M.F.P. Climate Change Will Affect the Asian Water Towers. *Science* **2010**, *328*, 1382–1385. [CrossRef]
10. Yao, T.; Bolch, T.; Chen, D.; Gao, J.; Immerzeel, W.; Piao, S.; Su, F.; Thompson, L.; Wada, Y.; Wang, L.; et al. The Imbalance of the Asian Water Tower. *Nat. Rev. Earth Environ.* **2022**, *3*, 618–632. [CrossRef]
11. Nie, Y.; Pritchard, H.D.; Liu, Q.; Hennig, T.; Wang, W.; Wang, X.; Liu, S.; Nepal, S.; Samyn, D.; Hewitt, K.; et al. Glacial Change and Hydrological Implications in the Himalaya and Karakoram. *Nat. Rev. Earth Environ.* **2021**, *2*, 91–106. [CrossRef]
12. O'Neel, S.; Marshall, H.P.; McNamara, D.E.; Pfeffer, W.T. Seismic Detection and Analysis of Icequakes at Columbia Glacier, Alaska. *J. Geophys. Res. Earth Surf.* **2007**, *112*, e2006JF000595. [CrossRef]
13. Roux, P.-F.; Marsan, D.; Métaxian, J.-P.; O'Brien, G.; Moreau, L. Microseismic Activity within a Serac Zone in an Alpine Glacier (Glacier d'Argentiere, Mont Blanc, France). *J. Glaciol.* **2008**, *54*, 157–168. [CrossRef]
14. Walter, F.; Deichmann, N.; Funk, M. Basal Icequakes during Changing Subglacial Water Pressures beneath Gornergletscher, Switzerland. *J. Glaciol.* **2008**, *54*, 511–521. [CrossRef]
15. Walter, F.; Roux, P.; Roeoesli, C.; Lecointre, A.; Kilb, D.; Roux, P.-F. Using Glacier Seismicity for Phase Velocity Measurements and Green's Function Retrieval. *Geophys. J. Int.* **2015**, *201*, 1722–1737. [CrossRef]
16. Röösli, C.; Walter, F.; Husen, S.; Andrews, L.C.; Lüthi, M.P.; Catania, G.A.; Kissling, E. Sustained Seismic Tremors and Icequakes Detected in the Ablation Zone of the Greenland Ice Sheet. *J. Glaciol.* **2014**, *60*, 563–575. [CrossRef]
17. Carmichael, J.D.; Joughin, I.; Behn, M.D.; Das, S.; King, M.A.; Stevens, L.; Lizarralde, D. Seismicity on the Western Greenland Ice Sheet: Surface Fracture in the Vicinity of Active Moulins. *J. Geophys. Res. Earth Surf.* **2015**, *120*, 1082–1106. [CrossRef]
18. Helmstetter, A.; Moreau, L.; Nicolas, B.; Comon, P.; Gay, M. Intermediate-Depth Icequakes and Harmonic Tremor in an Alpine Glacier (Glacier d'Argentière, France): Evidence for Hydraulic Fracturing? *J. Geophys. Res. Earth Surf.* **2015**, *120*, 402–416. [CrossRef]
19. Wittlinger, G.; Farra, V. Evidence of Unfrozen Liquids and Seismic Anisotropy at the Base of the Polar Ice Sheets. *Polar Sci.* **2015**, *9*, 66–79. [CrossRef]
20. Podolskiy, E.A.; Walter, F. Cryoseismology. *Rev. Geophys.* **2016**, *54*, 708–758. [CrossRef]
21. Roeoesli, C.; Walter, F.; Ampuero, J.-P.; Kissling, E. Seismic Moulin Tremor. *J. Geophys. Res. Solid Earth* **2016**, *121*, 5838–5858. [CrossRef]
22. Podolskiy, E.A.; Fujita, K.; Sunako, S.; Tsushima, A.; Kayastha, R.B. Nocturnal Thermal Fracturing of a Himalayan Debris-Covered Glacier Revealed by Ambient Seismic Noise. *Geophys. Res. Lett.* **2018**, *45*, 9699–9709. [CrossRef]
23. Chen, Y. Rule and affecting factors of seismic events in valley glacier with continental features: A case study on Laohugou Glacier No. 12. *J. Mar. Sci.* **2018**, *36*, 50–56.
24. Zhang, T.; Chen, Y.; Ding, M.; Shen, Z.; Yang, Y.; Guan, Q. Air-Temperature Control on Diurnal Variations in Microseismicity at Laohugou Glacier No. 12, Qilian Mountains. *Ann. Glaciol.* **2019**, *60*, 125–136. [CrossRef]
25. Zuo, H.; Pei, S.; He, J.; Sun, Q.; Xue, X.; Liu, Y.; Li, J.; Li, L. Research progress of the glacier seismology. *DQYXXWLPL* **2021**, *52*, 280–290. [CrossRef]
26. Daley, T.M.; Miller, D.E.; Dodds, K.; Cook, P.; Freifeld, B.M. Field Testing of Modular Borehole Monitoring with Simultaneous Distributed Acoustic Sensing and Geophone Vertical Seismic Profiles at Citronelle, Alabama. *Geophys. Prospect.* **2015**, *64*, 1318–1334. [CrossRef]
27. Liu, H.; Li, J.; Chi, B.X. Study of distributed acoustic sensing data waveform inversion based on strain rate. *Chin. J. Geophys.* **2022**, *65*, 3584–3598.
28. Zhang, H.; Tao, Z.; Huang, W.; Pei, S.; Nilot, E.; Li, Y.; Junmeng, Z. A New Application of Fiber Seismometer in the Yigong Lake, Tibetan Plateau. *Chin. J. Geophys.-Chin. Ed.* **2022**. [CrossRef]
29. Parker, L.M.; Thurber, C.H.; Zeng, X.; Li, P.; Lord, N.E.; Fratta, D.; Wang, H.F.; Robertson, M.C.; Thomas, A.M.; Karplus, M.S. Active-Source Seismic Tomography at the Brady Geothermal Field, Nevada, with Dense Nodal and Fiber-Optic Seismic Arrays. *Seismol. Res. Lett.* **2018**, *89*, 1629–1640. [CrossRef]
30. Yu, C.; Zhan, Z.; Lindsey, N.J.; Ajo-Franklin, J.B.; Robertson, M. The Potential of DAS in Teleseismic Studies: Insights from the Goldstone Experiment. *Geophys. Res. Lett.* **2019**, *46*, 1320–1328. [CrossRef]

31. Zeng, X.; Lancelle, C.; Thurber, C.; Fratta, D.; Wang, H.; Lord, N.; Chalari, A.; Clarke, A. Properties of Noise Cross-Correlation Functions Obtained from a Distributed Acoustic Sensing Array at Garner Valley, California. *Bull. Seismol. Soc. Am.* **2017**, *107*, 603–610. [CrossRef]
32. Lei, Y.; Yin, F.; Hong, H.; Li, Y.; Wang, B. Shallow Structure Imaging Using Higher-Mode Rayleigh Waves Based on FJ Transform in DAS Observation. *Chin. J. Geophys.* **2021**, *64*, 4280–4291.
33. Nayak, A.; Ajo-Franklin, J. Distributed Acoustic Sensing Using Dark Fiber for Array Detection of Regional Earthquakes. *Seismol. Res. Lett.* **2021**, *92*, 2441–2452. [CrossRef]
34. Booth, A.D.; Christoffersen, P.; Schoonman, C.; Clarke, A.; Hubbard, B.; Law, R.; Doyle, S.H.; Chudley, T.R.; Chalari, A. Distributed Acoustic Sensing of Seismic Properties in a Borehole Drilled on a Fast-Flowing Greenlandic Outlet Glacier. *Geophys. Res. Lett.* **2020**, *47*, e2020GL088148. [CrossRef]
35. Paitz, P.; Edme, P.; Gräff, D.; Walter, F.; Doetsch, J.; Chalari, A.; Schmelzbach, C.; Fichtner, A. Empirical Investigations of the Instrument Response for Distributed Acoustic Sensing (DAS) across 17 Octaves. *Bull. Seismol. Soc. Am.* **2020**, *111*, 1–10. [CrossRef]
36. Walter, F.; Gräff, D.; Lindner, F.; Paitz, P.; Köpfli, M.; Chmiel, M.; Fichtner, A. Distributed Acoustic Sensing of Microseismic Sources and Wave Propagation in Glaciated Terrain. *Nat. Commun.* **2020**, *11*, 2436. [CrossRef]
37. Hudson, T.S.; Baird, A.F.; Kendall, J.M.; Kufner, S.K.; Brisbourne, A.M.; Smith, A.M.; Butcher, A.; Chalari, A.; Clarke, A. Distributed Acoustic Sensing (DAS) for Natural Microseismicity Studies: A Case Study From Antarctica. *J. Geophys. Res. Solid Earth* **2021**, *126*, e2020JB021493. [CrossRef]
38. Zhou, W.; Butcher, A.; Brisbourne, A.M.; Kufner, S.-K.; Kendall, J.-M.; Stork, A.L. Seismic Noise Interferometry and Distributed Acoustic Sensing (DAS): Inverting for the Firn Layer S-Velocity Structure on Rutford Ice Stream, Antarctica. *J. Geophys. Res. Earth Surf.* **2022**, *127*, e2022JF006917. [CrossRef]
39. Ding, J.; Jiang, H. Seismic scattering technology and its application in goaf exploration. *Prog. Geophys.* **2015**, *30*, 1459–1464.
40. Jiang, H.; Liu, C.; Jia, C.; Hou, J. The application of seismic scattering technology to detection of grouting effect. *Chin. J. Eng. Geophys.* **2015**, *12*, 260–265.
41. Jiang, D.; Zhang, W.; Li, F. All-Metal Optical Fiber Accelerometer With Low Transverse Sensitivity for Seismic Monitoring. *Sens. J. IEEE* **2013**, *13*, 4556–4560. [CrossRef]
42. Huang, W.; Zhang, W.; Huang, J.; Li, F. Demonstration of Multi-Channel Fiber Optic Interrogator Based on Time-Division Locking Technique in Subway Intrusion Detection. *Opt. Express* **2020**, *28*, 11472–11481. [CrossRef] [PubMed]
43. Millan, R.; Mouginot, J.; Rabatel, A.; Morlighem, M. Ice Velocity and Thickness of the World's Glaciers. *Nat. Geosci.* **2022**, *15*, 124–129. [CrossRef]
44. Mikesell, T.D.; van Wijk, K.; Haney, M.M.; Bradford, J.H.; Marshall, H.-P.; Harper, J.T. Monitoring Glacier Surface Seismicity in Time and Space Using Rayleigh Waves. *J. Geophys. Res. Earth Surf.* **2012**, *117*, F02020. [CrossRef]
45. Neave, K.G.; Savage, J.C. Icequakes on the Athabasca Glacier. *J. Geophys. Res.* **1970**, *75*, 1351–1362. [CrossRef]
46. Deichmann, N.; Ansorge, J.; Scherbaum, F.; Aschwanden, A.; Bernard, F.; Gudmundsson, G.H. Evidence for Deep Icequakes in an Alpine Glacier. *Ann. Glaciol.* **2000**, *31*, 85–90. [CrossRef]
47. West, M.; Larsen, C.; Truffer, M.; O'Neel, S.; LeBlanc, L. Glacier Microseismicity. *Geology* **2010**, *38*, 319–322. [CrossRef]
48. Walter, F.; Dalban Canassy, P.; Husen, S.; Clinton, J.F. Deep Icequakes: What Happens at the Base of Alpine Glaciers? *J. Geophys. Res. Earth Surf.* **2013**, *118*, 1720–1728. [CrossRef]
49. Helmstetter, A.; Nicolas, B.; Comon, P.; Gay, M. Basal Icequakes Recorded beneath an Alpine Glacier (Glacier d'Argentière, Mont Blanc, France): Evidence for Stick-Slip Motion? *J. Geophys. Res. Earth Surf.* **2015**, *120*, 379–401. [CrossRef]
50. Kohnen, H. The Temperature Dependence of Seismic Waves in Ice. *J. Glaciol.* **1974**, *13*, 144–147. [CrossRef]
51. Llorens, M.-G.; Griera, A.; Bons, P.D.; Weikusat, I.; Prior, D.J.; Gomez-Rivas, E.; de Riese, T.; Jimenez-Munt, I.; García-Castellanos, D.; Lebensohn, R.A. Can changes in deformation regimes be inferred from crystallographic preferred orientations in polar ice? *Cryosphere* **2022**, *16*, 2009–2024. [CrossRef]
52. Llorens, M.G.; Griera, A.; Bons, P.D.; Weikusat, I.; Prior, D.; Gomez-Rivas, E.; de Riese, T.; Jimenez-Munt, I.; García Castellanos, D.; Lebensohn, R.A. Can Changes in Ice-Sheet Flow Be Inferred from Crystallographic Preferred Orientations?; Ice sheets/Numerical Modelling: 2021. *Cryosphere Discuss.* **2021**, *2021*, 1–24.
53. Zhang, T.; Ding, M.; Xiao, C.; Zhang, D.; Du, Z. Temperate Ice Layer Found in the Upper Area of Jima Yangzong Glacier, the Headstream of Yarlung Zangbo River. *Sci. Bull.* **2016**, *61*, 619–621. [CrossRef]
54. Meyer, C.R.; Minchew, B.M. Temperate Ice in the Shear Margins of the Antarctic Ice Sheet: Controlling Processes and Preliminary Locations. *Earth Planet. Sci. Lett.* **2018**, *498*, 17–26. [CrossRef]
55. Gilbert, A.; Sinisalo, A.; Gurung, T.R.; Fujita, K.; Maharjan, S.B.; Sherpa, T.C.; Fukuda, T. The Influence of Water Percolation through Crevasses on the Thermal Regime of a Himalayan Mountain Glacier. *Cryosphere* **2020**, *14*, 1273–1288. [CrossRef]
56. Nanni, U.; Gimbert, F.; Roux, P.; Lecointre, A. Observing the Subglacial Hydrology Network and Its Dynamics with a Dense Seismic Array. *Proc. Natl. Acad. Sci. USA* **2021**, *118*, e2023757118. [CrossRef]
57. Nanni, U.; Roux, P.; Gimbert, F.; Lecointre, A. Dynamic Imaging of Glacier Structures at High-Resolution Using Source Localization With a Dense Seismic Array. *Geophys. Res. Lett.* **2022**, *49*, e2021GL095996. [CrossRef]
58. Van der Veen, C.J. Fracture Mechanics Approach to Penetration of Surface Crevasses on Glaciers. *Cold Reg. Sci. Technol.* **1998**, *27*, 31–47. [CrossRef]

59. van der Veen, C.J. Fracture Propagation as Means of Rapidly Transferring Surface Meltwater to the Base of Glaciers. *Geophys. Res. Lett.* **2007**, *34*, L01501. [CrossRef]
60. Carmichael, J.D.; Pettit, E.C.; Hoffman, M.; Fountain, A.; Hallet, B. Seismic Multiplet Response Triggered by Melt at Blood Falls, Taylor Glacier, Antarctica. *J. Geophys. Res. Earth Surf.* **2012**, *117*, F03004. [CrossRef]
61. Colgan, W.; Rajaram, H.; Abdalati, W.; McCutchan, C.; Mottram, R.; Moussavi, M.S.; Grigsby, S. Glacier Crevasses: Observations, Models, and Mass Balance Implications. *Rev. Geophys.* **2016**, *54*, 119–161. [CrossRef]